Suppression of secondary electrons from an endplate of a tandem mirror by use of a biased mesh

doi: 10.1063/1.871439

Suppression of secondary electrons from an endplate of a tandem mirror by use of a biased mesh

T. Saito, Y. Kiwamoto, Y. Tatematsu, Y. Yoshimura, T. Takahashi, M. Inutake,[a] and T. Tamano
Plasma Research Center, University of Tsukuba, Tsukuba City, Ibaraki 305, Japan

(Received 1 August 1994; accepted 17 October 1994)

Negative bias is applied to a mesh placed in front of an endplate of the GAMMA 10 tandem mirror [Phys. Rev. Lett. **55**, 939 (1985)]. A bias voltage of around 10 V results in an increase of the potential difference by an order of kV in the end region. The increment is about two times the temperature of end-loss electrons and most of that stems from the sheath potential drop in front of the endplate. Provided that almost all the secondary electrons emitted from endplate are reflected, these results agree with the prediction of a potential model for the open magnetic field configuration [J. Phys Soc. Jpn. **61**, 3153 (1992)]. © *1995 American Institute of Physics.*

Secondary electron emission (SEE) from plasma facing materials strongly affects energy flow to walls as well as the potential distribution in the edge region.[1] Moreover, SEE is an important factor for energy confinement in a tandem mirror because cold secondary electrons flow back to the confinement region along magnetic field lines and replace heated electrons. Thus, examination of effects of SEE is one of key tasks in the study of mirror fusion. Theoretically, degradation of energy confinement due to SEE has been discussed in several papers[2,3] and use of a biased mesh has been pointed out as one of the promising methods to suppress SEE. Also, an idea of a thermal dike has recently been proposed to reduce the cold electron flow to the confinement region.[4] However, suppression of SEE has only been tested by using a picket fence of permanent magnets in a laboratory plasma.[5]

This paper describes the first results of suppression of SEE by using a mesh placed on an endplate of GAMMA 10 (Ref. 6) and examines the dependence of the potential in the end region on the bias voltage. Figure 1 shows the potential profile expected in GAMMA 10. When electron cyclotron resonance heating at the plug is applied, an intense end-loss electron flux of hundreds of eV to several keV is generated[7,8] and the endplate potential Φ_{EP} goes down.[9] The end-loss electrons induce secondary electrons from the endplate.[10] The potential profile outside the mirror throat is predicted by a potential model including the experimental conditions.[11] The energy spectrum of the end-loss electrons is expressed by a Maxwellian of two temperatures T_{eL} and T_{eH}. The model takes account of the secondary electrons and the magnetic field profile. Collisions are neglected and distribution functions of each species satisfy the Vlasov equation. The floating condition of the endplate determines the potential difference $\Delta\Phi$ as shown in Fig. 1. It has been confirmed that the experimental value of $\Delta\Phi$ is well reproduced by this model.[12]

The potential model gives the following expression to the end-loss electron flux Γ_e:

$$\Gamma_e = N_{e0}\left(\frac{T_e}{2\pi m_e}\right)^{1/2}\left[\exp\left(-\frac{e\Phi_{MP}}{T_e}\right) - \left(\frac{B_{Th}-B_{EP}}{B_{Th}}\right)\exp\left(-\frac{B_{Th}}{B_{Th}-B_{EP}}\frac{e\Phi_{MP}}{T_e}\right)\right]. \quad (1)$$

Here, N_{e0} is the density of the end-loss electrons at the mirror throat and T_e is the electron temperature. The magnetic field strengths at the mirror throat and at the endplate are denoted by B_{Th} and B_{EP}. The potential at the mirror throat measured from the endplate is represented by Φ_{MP}. According to the model Φ_{MP} increases with decreasing SEE coefficient γ. The primary function of the mesh biasing is reduction of the heat loss to the endplate by suppressing SEE. Thus, we have to examine the response of the potential difference to the bias voltage. Moreover, mesh biasing confirms the effects of secondary electrons on the potential profile in an open system.

The confinement region of the GAMMA 10 device consists of the central cell, two anchor cells, and two end mirror cells. Outside the confinement region, the end region expands toward the endplate. The outer mirror throat of the end mirror cell connects the confinement region with the end region. The value of B_{Th} is 0.3 T and that of B_{EP} is 0.01 T. The endplate consists of five annular rings.[13] Each piece of the plates is made of stainless steel and connected to the machine ground through a high resistance. Negative voltage is applied to a mesh placed in front of the innermost plate (#1 plate, 3650 cm^2). A stainless steel mesh with 50 grids of 50 μm diameter wire per inch is used. The transparency of the mesh is more than 80%. The distance between the endplate and the mesh is 2 cm. The bias circuit is floated from the machine ground and the reference of the bias is the endplate.

The potentials at the central cell Φ_C and at the barrier midplane Φ_B are measured by gold beam probes.[14] The plug potential Φ_P is evaluated from the energy spectrum of the end-loss ions. Two Langmuir probes shown in Fig. 1 are used to obtain the space potentials Φ_I and Φ_O in the end region. The energy spectrum of the end-loss electrons is obtained with a multigrid energy analyzer called an LED (loss electron diagnostic).

The response of the measured potentials to the mesh bias V_M is shown in Fig. 2. Here, V_M is the voltage between the mesh and the endplate. The bias circuit has a series resistance R_s of 100 Ω and the circuit current I_c is monitored. The supply voltage V_s necessary to support V_M is $V_M + I_c R_s$. On-axis values are plotted for Φ_C, Φ_B, and Φ_P. All the plotted potentials are referenced to the machine

 1070-664X/95/2(2)/352/3/$6.00

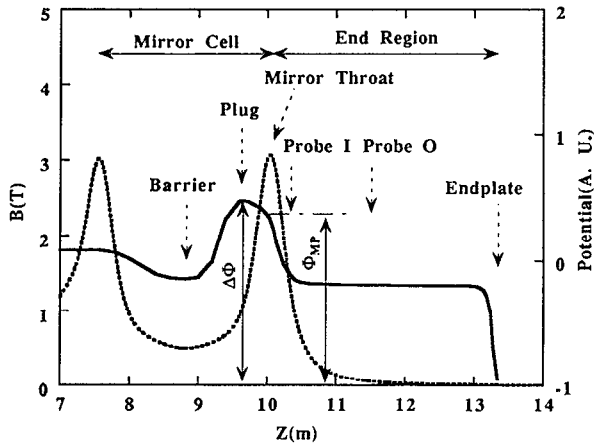

FIG. 1. Axial profiles of the magnetic field strength (dashed line) and the potential (solid line) in the end mirror cell and the end region. The potential profile in the end region corresponds to the calculated profile from the potential model. The origin of the z axis is located at the midplane of the central cell. The arrows except at the mirror throat indicate the positions of potential measurement.

ground. The floating potential Φ_{EP} promptly descends with V_M and then saturates at V_M of 20–30 V. Typical value of I_c is 0.5 A at V_M of 20 V. This behavior of Φ_{EP} is understood if all the secondary electrons with a mean energy of around 10 eV are reflected to the endplate by the mesh. The floating potential descends to reflect end-loss electrons on way to the endplate. Consequently, the net current flowing to the endplate is kept to be zero with reduced SEE.

Contrary to the behavior of Φ_{EP}, other potentials do not vary with V_M. Figure 3 plots the axial potential profile along the magnetic field line which passes the #1 plate for three representative values of V_M. The difference between Φ_O and Φ_{EP} stands for the sheath potential drop Φ_{sheath} in front of the endplate and Fig. 3 indicates that most of the increment of $\Delta\Phi \equiv \Phi_P - \Phi_{EP}$ stems from the increase of Φ_{sheath}. From the viewpoint of the axial charge balance, only an increase of

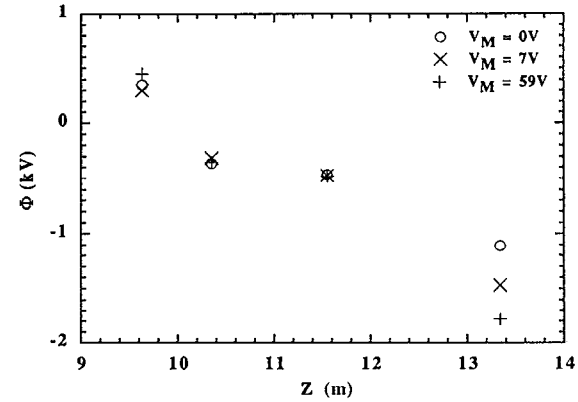

FIG. 3. Axial potential profiles for three representative values of V_M. In this figure are plotted potentials on the magnetic field line which passes the #1 plate.

$\Delta\Phi$ is required. Therefore, it is also possible that both Φ_P and Φ_{EP} vary and results in the same $\Delta\Phi$. However, this is not the case in the present experiment.

The potential model predicts the response of the axial potential profile to variation of the SEE coefficient γ. Figure 4 plots the calculated potentials corresponding to the plug, the probe position, and the endplate as functions of γ. In the model the potential is referred to be zero at the mirror throat and normalized by the temperature T_{eL} of the bulk component of the end-loss electrons.

This model does not determine the potential as measured from the vacuum vessel. However, once we acknowledge the absolute value of the potential at each point for no bias as the initial one, the model explains the observed response of the potentials to V_M. Figure 4 states that the potential difference $\Delta\Phi_1 \equiv (\Psi_P - \Psi_S) \times T_{eL}$ from the plug to the probe position is determined essentially independent of SEE. It is mainly determined from the dynamics of the end-loss ions and the end-loss electrons according to the rapid decrease of the

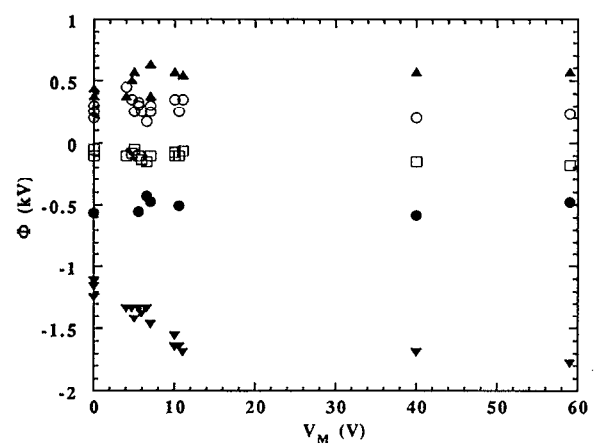

FIG. 2. Response of the potentials Φ_P (▲), Φ_C (○), Φ_B (□), Φ_O (●), and Φ_{EP} (▼) to the voltage V_M between the mesh and the endplate. The mesh voltage is negative to the endplate. Here, on-axis values are plotted by Φ_C, Φ_B, and Φ_P.

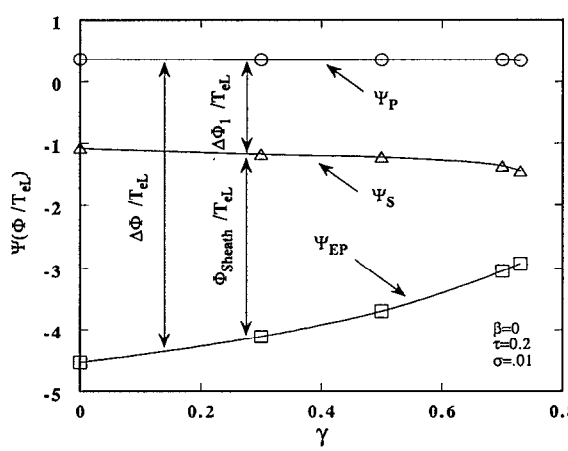

FIG. 4. The normalized potentials calculated by the model are plotted as functions of the secondary electron emission coefficient γ. The potential at the mirror throat is referred to be zero in the model. The difference $\Psi_P - \Psi_{EP}$ corresponds to $\Delta\Phi/T_{eL}$ and $\Psi_S - \Psi_{EP}$ denotes Φ_{sheath}/T_{eL}, where, $\Delta\Phi = \Phi_P - \Phi_{EP}$ and $\Phi_{sheath} = \Phi_O - \Phi_{EP}$.

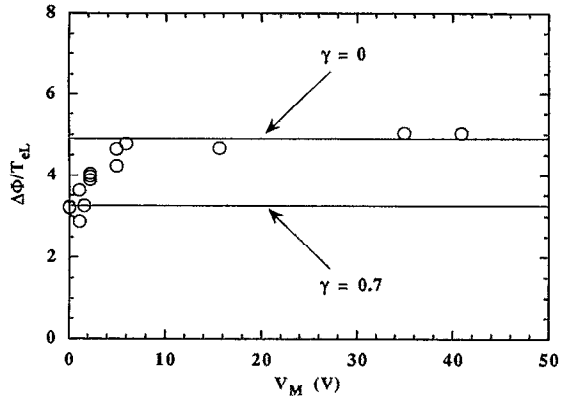

FIG. 5. Normalized potential difference $\Delta\Phi/T_{eL}$ is shown as a function of V_M.

magnetic field strength outside the mirror throat. The secondary electron density is much smaller in the confinement region than at the probe position and hence the potentials in the confinement region are determined independent of SEE from the endplate. Thus the plug potential Φ_P does not vary with V_M. On the other hand, the model provides the total difference $\Delta\Phi$ and the apportion between $\Delta\Phi_1$ and Φ_{sheath}. The only way to meet all the above restrictions is as shown in Fig. 3.

Next we compare the measured increment of $\Delta\Phi$ with that of the calculation. Figure 5 plots $\Delta\Phi/T_{eL}$ as a function of V_M. The value of T_{eL} does not change very much with V_M. The normalized potential difference quickly increases with V_M from around 3 and then saturates at about 5. The quantity $\Delta\Phi/T_{eL}$ compares with $\Psi_P-\Psi_{EP}$ shown in Fig. 4, which also varies from 3 to 5 with decreasing γ. Thus, the experimentally observed value is consistent with the calculated value if all the secondary electrons are reflected at V_M larger than 20–30 V and γ is regarded as zero.

In this experiment only the #1 plate is covered by the mesh and SEE from the outer plates is not controlled. The measured floating potentials of the outer plates do not vary when a bias voltage is applied to the mesh. This means that the predominant factor determining the potential profile along each magnetic field line is the axial dynamics of end-loss particles. This also supports the application of the model which takes only the axial dynamics of the particles into account.

The increase of $\Delta\Phi$ reduces the loss power density W to the endplate. The potential model gives the following expression of W:

$$W=\Gamma_i(2T_i+e\Delta\Phi)+2\Gamma_e T_e. \tag{2}$$

The ion flux is denoted by Γ_i and the electron flux Γ_e is given by Eq. (1). Contribution of the secondary electrons is neglected. Equation (2) is essentially the same formula as given in Ref. 3. However, the end-loss electrons have two components in GAMMA 10 and T_e should be replaced by $T_{\text{eff}}=(1-\beta)T_{eL}+\beta T_{eH}$. Here, β is the flux fraction of the higher temperature component. The difference between W with bias and that without bias is

$$\delta W=[\Gamma_i e\,\delta\Phi+2T_{\text{eff}}(\Gamma_{e,\text{bias}}-\Gamma_{e,0})]. \tag{3}$$

Here, $\delta\Phi$ is the increment of $\Delta\Phi$. When SEE from the endplate is suppressed, the relation $\Gamma_i=\Gamma_{e,\text{bias}}$ holds. From the experiment, $e\,\delta\Phi$ is nearly equal to T_{eff} and $\Gamma_{e,0}=(2-3)\times\Gamma_{e,\text{bias}}$. Hence the positive ion term is masked by the negative electron term. Because Φ_{MP} increases by $\delta\Phi$, reduction of Γ_e can be estimated by using Eq. (1) if N_{e0} and T_e do not change. In fact, N_{e0} and T_e may vary by mesh biasing. Moreover, the end-loss electrons have two components. Therefore, we use the experimentally observed values. The total electron flux measured by the LED decreases from 8.7×10^{-4} A/cm^2 to 4.2×10^{-4} A/cm^2. The value of T_{eff} slightly increases from 0.5 to 0.6 keV. Thus δW is estimated to be about 0.37 W/cm^2. If we simply multiply this value by the area of the #1 plate, decrement of the loss power to the #1 plate is 1.3 kW per one end. On the other hand, the power $V_s I_c$ dissipated in the bias circuit is equal to 70 V×0.5 A=0.035 kW, which is much less than the above value.

A negatively biased mesh suppresses secondary electrons emitted from the endplate and increases the sheath potential drop in front of the endplate. The potential drop reduces the loss power to the endplate with a very low cost of bias power. Though a material mesh may work only in an experiment with low power density, the present study demonstrates the effectiveness of suppressing backward flow of colder electrons for decreasing electron heat load to end walls. For larger experiment, thermal dike, e.g., is a possible candidate to be studied next.[15,16]

[a]Permanent address: Department of Electrical Engineering, Faculty of Engineering, Tohoku University, Sendai, Japan.

[1]P. C. Stangeby, in *Physics of Plasma–Wall Interactions in Controlled Fusion*, NATO ASI Series B-131, edited by D. E. Post and R. Behrisch (Plenum, New York, 1984), p. 41.
[2]L. S. Hall, Nucl. Fusion **17**, 681 (1977).
[3]G. D. Porter, Nucl. Fusion **22**, 1279 (1982).
[4]T. Ohkawa, Kakuyugo-Kenkyuu (J. Plasma Fusion Res.) **64**, 305 (1990).
[5]C. Chan, H. Bewley, N. Hershkowitz, and J. R. Dekock, Nucl. Fusion **22**, 105 (1982).
[6]M. Inutake, T. Cho, M. Ichimura, K. Ishii, A. Itakura, I. Katanuma, Y. Kiwamoto, Y. Kusama, A. Mase, S. Miyoshi, Y. Nakashima, T. Saito, A. Sakasai, K. Sawada, I. Wakaida, N. Yamaguchi, and K. Yatsu, Phys. Rev. Lett. **55**, 939 (1985).
[7]T. Karyia, T. Saito, Y. Kiwamoto, T. Cho, H. Sugawara, T. Kondoh, A. Mase, A. Itakura, and S. Miyoshi, Phys. Fluids **31**, 1815 (1988).
[8]Y. Kiwamoto, T. Saito, I. Katanuma, K. Kurihara, and S. Miyoshi, J. Phys. Soc. Jpn. **58**, 2619 (1989).
[9]T. Saito, K. Kiwamoto, K. Kurihara, T. Honda, A. Kasugai, T. Cho, K. Ishii, I. Katanuma, A. Mase, Y. Yamaguchi, and S. Miyoshi, in *Strong Microwaves in Plasmas* (Institute of Applied Physics, Nizhniy Novgorod, 1991), Vol. 1, p. 165.
[10]K. Kurihara, T. Saito, Y. Kiwamoto, and S. Miyoshi, J. Phys. Soc. Jpn. **58**, 3453 (1989).
[11]K. Kurihara, Y. Kiwamoto, T. Saito, K. Yatsu, and S. Miyoshi, J. Phys. Soc. Jpn. **61**, 3153 (1992).
[12]T. Saito, Y. Kiwamoto, K. Kurihara, T. Cho, M. Inutake, S. Miyoshi, T. Tamano, and K. Yatsu, Phys. Fluids B **5**, 866 (1993).
[13]I. Katanuma, Y. Kiwamoto, S. Adachi, M. Inutake, K. Ishii, K. Yatsu, K. Sawada, and S. Miyoshi, Nucl. Fusion **27**, 2041 (1987).
[14]K. Ishii, M. Kotoku, T. Segawa, I. Katanuma, A. Mase, and S. Miyoshi, Rev. Sci. Instrum. **60**, 3270 (1989).
[15]Y. Tatematsu, Y. Kiwamoto, T. Saito, and T. Tamano, J. Phys. Soc. Jpn. **63**, 558 (1994).
[16]Y. Kiwamoto, T. Tatematsu, T. Saito, I. Katanuma, Y. Yoshimura, and T. Tamano, Phys. Plasmas **1**, 3986 (1994).